Rhenium Complex with Noninnocent Dioxolene Ligand: Combined Experimental and ab Initio Study of [(3,5-di- tert -Bu 2 C 6 H 2 O 2)ReCl 3 (OPPh 3)]

ARTICLE *in* INORGANIC CHEMISTRY · JULY 2015

Impact Factor: 4.76 · DOI: 10.1021/acs.inorgchem.5b00407 · Source: PubMed

Inorganic Chemistry

Article

pubs.acs.org/IC

Rhenium Complex with Noninnocent Dioxolene Ligand: Combined Experimental and ab Initio Study of [(3,5-di-*tert*-$Bu_2C_6H_2O_2$)$ReCl_3(OPPh_3)$]

Pavel A. Abramov,*[,†,‡] Nina P. Gritsan,*[,‡,§] Elizaveta A. Suturina,[‡,§] Artem S. Bogomyakov,[‡,∥] and Maxim N. Sokolov[†,‡]

[†]Nikolayev Institute of Inorganic Chemistry, Prospekt Lavrentyeva 3, 630090 Novosibirsk, Russia

[‡]Novosibirsk State University, Pirogova str. 2, 630090 Novosibirsk, Russia

[§]Voevodsky Institute of Chemical Kinetics and Combustion, Institutskaya str. 3, 630090 Novosibirsk, Russia

[∥]International Tomography Center, Institutskaya str. 3a, 630090 Novosibirsk, Russia

Supporting Information

ABSTRACT: Reaction of $[ReOCl_3(PPh_3)_2]$ with 3,5-di-*tert*-butyl-1,2-benzoquinone (3,5-DTBQ) in hot toluene produces a new complex [(3,5-di-*tert*-$Bu_2C_6H_2O_2$)$Re(OPPh_3)Cl_3$] (**1**), which was isolated and characterized by elemental analysis, IR, UV−vis spectroscopy, and cyclic voltammetry. In order to clarify the charge state of rhenium and the coordinated dioxolene ligand, X-ray experiments at 150 and 290 K were carried out. The C−O, C−C, and Re−O bond distances at both 150 and 290 K fall between those for semiquinolate (3,5-DTBSQ) and catecholate (3,5-DTBCat) forms; an empirical "metrical oxidation state" of the dioxolene ligand was estimated to be −1.5. High-level *ab initio* calculations (SOC-CASSCF/NEVPT2) revealed a mixed valence nature of the triplet ground state of complex **1** corresponding to a superposition of the Re^{IV}−*SQ* and Re^{V}−*cat* forms. In agreement with the high-level *ab initio* and DFT calculations, the temperature dependence of the magnetic susceptibility (5−300 K) is well described in the assumption of the triplet ground state, with the anomalously large zero-field splitting (ZFS) arising from the spin−orbit coupling. According to the *ab initio* calculations, all absorption bands in the visible region of the electronic absorptions spectrum are assigned to the LMCT bands, with significant contribution of the intraligand transition in the most intense band at 555 nm.

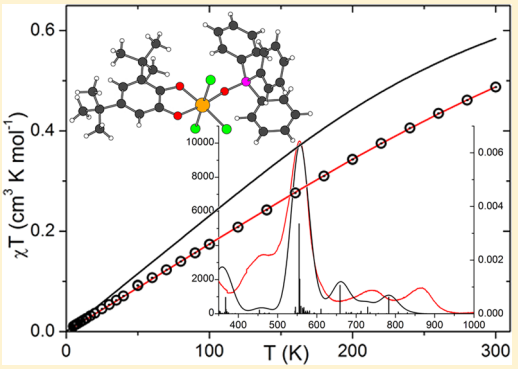

INTRODUCTION

Transition metal complexes with stable organic radicals and radical anions are of great importance as potential building blocks of molecular magnetic materials[1] as well as models of the active sites of metalloproteins.[2] Of particular interest are transition metal complexes of noninnocent redox active ligands which are the objects of intense research in the fields of inorganic and bioinorganic chemistry[3] due to their catalytic activity,[4] biological importance, and unusual magnetic properties.[5] A hot topic in this broad area of inorganic chemistry is understanding the bonding and physical properties of these complexes.[6]

The dioxolene type ligands derived from *ortho*-quinones, namely the catecholates (Cat, dianionic), *o*-semiquinone radical anions (SQ, monoanionic), and *o*-quinones (Q, neutral), attract the most attention due to their versatile structural,[7] magnetochemical,[5] spectral,[8] electrochemical,[9] and chemical properties.[7] Formation of the intensively colored complexes in the reaction of metal halides with *o*-quinines was discovered at the beginning of the last century.[10] The study of such complexes was resumed only in the early 1960s,[11] and the first metal complexes with *o*-semiquinone type radical anions were detected using EPR.[12] Since then, a large series of complexes with early transition metals (Ti, V, Mn, Cr, Fe, Co, Ni) with dioxolene type ligands has been thoroughly studied and created the base for further work in this field.[13] Besides that, complexes of Cu and Ru came into the focus, producing the first polynuclear complexes with dioxolene ligands.[14] However, second and third row (4*d*-, 5*d*-) transition metals remained in the shadow for a long time. Among these, rhenium is particularly well suited for coordination of such ligands, since it is sufficiently oxophilic and displays a wide range of accessible and stable oxidation states, which favors noninnocent behavior. According to the literature, with 3,5-di-*tert*-butyl-1,2-benzoquinone (3,5-DTBQ), Re can form both semiquinolate (in $[Re(CO)_3(PPh_3)$(3,5-DTBSQ)$]$[15,16]) and catecholate (in $(NEt_4)[ReO_2$(3,5-DTBCat)$_2]$,[17] $(NEt_4)[ReO$(3,5-

Received: February 21, 2015
Published: July 2, 2015

DOI: 10.1021/acs.inorgchem.5b00407
Inorg. Chem. 2015, 54, 6727−6735

DTBCat)$_2$],[18] and [Re(3,5-DTBCat)$_3$]^{19}) type complexes. To the best of our knowledge, only a few examples of Re(IV) complexes with dioxolene-type ligands have been reported.[20,21] The magnetic properties were measured only for the $[Re^{IV}Cl_4(Cat)]^{2-}$ complex; they correspond to the quartet ground state ($S = {}^3/_2$) with enough large zero-field splitting (ZFS) ($|2D| = 190$ cm^{-1}).[21a] Only one complex of Re(IV) with a natural 1,2-naphthoquinone derivative, β-lapachone, was synthesized and assigned to the semiquinolate-type complex. This assignment was based only on the XRD data analysis.[20] However, it should be noted that complexes containing a dioxolene ligand coordinated to a redox active metal may exist not only as the valence-localized structures discussed above, *viz.* $M^{(n+2)+} - Cat$ or $M^{(n+1)+} - SQ$, but also as delocalized $[M(Diox)]^{n+}$ complexes.[9,22] As a measure of the delocalization, an empirical "metrical oxidation state" (MOS) of the noninnocent redox-active ligands has been recently proposed.[23]

In this work we report on a new rhenium complex (formally Re^{IV}) with the dioxolene-type ligand. In contrast to the previous study,[20] a detailed analysis of the electronic structure, magnetic properties, and charge and spin distribution between rhenium ion and dioxolene ligand has been performed based on the X-ray structural analysis data, cyclic voltammetry, magnetic measurements, electronic absorption, and IR spectroscopies coupled with quantum chemical calculations. Understanding the electronic structure of such systems is a nontrivial problem that can only be solved using both a large set of experimental techniques and comparison of their results with quantum chemical calculations. The density functional theory has been used most exclusively to calculate the properties of the metal complexes with potentially noninnocent ligands.[6d,22−24] On the other hand, more sophisticated theoretical models may be required to describe the properties of such complicated systems.[23,25] Moreover, in the case of rhenium complexes, the relativistic effects must be correctly taken into account. Thus, in this paper, we relied primarily on the results of the multireference CASSCF/NEVPT2 calculations with nonperturbative account of the spin−orbit coupling. Nevertheless, the DFT results and their comparison with the results of more sophisticated calculations are briefly discussed.

EXPERIMENTAL AND COMPUTATIONAL DETAILS

General Information. $[ReOCl_3(PPh_3)_2]$ was prepared according to the previously published procedure.[26] All solvents were purified by the standard methods. IR spectra were recorded on a Scimitar FTS 2000 (room temperature) and a Bruker Vertex 80 spectrometers (VT-FTIR experiments). Elemental analysis was carried out on a Eurovector EA 3000 CHN analyzer. The electronic absorption spectrum in dichloromethane solution was recorded on a Helios γ UV−vis spectrometer.

*Synthesis of [(3,5-SQ)Re(OPPh$_3$)Cl$_3$] (**1**).* A mixture of 0.10 g (0.12 mmol) $[ReOCl_3(PPh_3)_2]$ and 0.025 g of 3,5-DTBQ (0.12 mmol) in 10 mL of toluene was refluxed overnight until the solution turned purple. The solution was concentrated by pumping off the solvent and subjected to column chromatography on SiO_2. After washing with toluene (a small amount of unidentified dark purple product came out) the product was eluted with 1:1 v/v toluene: EtOH mixture. After evaporation of the solvent, the solid was extracted into 5 mL of CH_2Cl_2 and again purified by column chromatography on SiO_2 with CH_2Cl_2 as eluent (single band). The final solution was reduced in volume to 5 mL, placed into a 50 mL round flask and allowed to free evaporation in air that gives needle-like single crystals of **1**. Yield 60%. Calc. for $ReO_3PC_{32}H_{35}Cl_3$ (%) C 48.6, H 4.5. Found C 49.0, H 5.0. IR (KBr, cm^{-1}) 3058(w), 2966(m), 1577(w), 1438(s), 1126(vs), 1079(vs), 1026(m), 997(m), 727(s), 691(s), 532(s). The complex is ESR silent between 298 and 4 K. ^{31}P NMR ($CDCl_3$, r.t., δ, ppm): 32 (width 35 Hz).

X-ray Crystallography. The data collection was performed on a Bruker Apex II (room temperature, Mo Kα) and Bruker Apex Duo (150 K, Mo Kα) diffractometers (details of X-ray experiments and refinement are summarized in Table S3). The structures were solved by direct methods and refined by full matrix least-squares on $|F^2|$ with SHELX program set.[27] All the non-hydrogen atoms were treated anisotropically. The hydrogen atoms were placed in the calculated positions with isotropic displacement parameters set to 1.2 Ueq of the attached atom. The crystallographic data have been deposed in the Cambridge Crystallographic Data Center under the deposition code CCDC 876971(r.t.) and CCDC 1407244(l.t.).

Cyclic Voltammetry. CV experiments were performed with an electrochemical analyzer 797 VA Computrance (Metrohm, Switzerland). A three-electrode 10 mL glass cell was used. A platinum wire (Metrohm, Switzerland) and Ag/AgCl electrode filled with saturated KCl solution (+0.022 V vs NHE) served as counter and reference electrodes, respectively. Working electrode was glassy carbon.

Magnetic Measurements. The magnetic susceptibility of the polycrystalline sample was measured with a Quantum Design MPMSXL SQUID magnetometer in the temperature range 5−300 K with magnetic field of up to 5 kOe. The complex did not exhibit any field dependence of molar magnetization at low temperatures. Diamagnetic corrections were made using the Pascal constants.[28]

Simulation of Magnetic Susceptibility Temperature Dependences. The temperature dependence of the magnetic susceptibility has been fitted using julX program (version 1.4.1).[29]

Two models were used to simulate temperature dependences of the molar magnetic susceptibility. In the first model, the spin-Hamiltonian 1 assuming two spin centers: $S(Re^{IV}) = {}^3/_2$ with zero-field splitting (ZFS) and $S(SQ) = {}^1/_2$ connected by exchange interaction was employed:

$$\hat{H}_1 = -2J\hat{\vec{S}}_{Re^{IV}}\hat{\vec{S}}_{SQ} + D\hat{S}_{Re^{IV}z}^2 + E(\hat{S}_{Re^{IV}x}^2 - \hat{S}_{Re^{IV}y}^2) + g_{Re^{IV}}\beta\vec{H}\hat{\vec{S}}_{Re^{IV}} + g_{SQ}\beta\vec{H}\hat{\vec{S}}_{SQ} \quad (1)$$

In the second model, the spin-Hamiltonian in eq 2, assuming only a spin center with the spin $S = 1$ and ZFS, was employed:

$$\hat{H}_2 = D\hat{S}_z^2 + E(\hat{S}_x^2 - \hat{S}_y^2) + g\beta\vec{H}\hat{\vec{S}} \quad (2)$$

Computational Details. The ORCA[30] computational package was employed for most of quantum chemical calculations. The state-averaged (SA) CASSCF/NEVPT2 procedure[31] was used for the calculation of the wave functions of spin-free states. The scalar relativistic effects were taken into account using standard second-order Douglas−Kroll−Hess[32] (DKH2) procedure. Relativistically recontracted versions of the def2-TZVP basis sets (for atoms H − Ba)[33] and all-electron relativistically contracted (SARC) basis set of the same quality for rhenium[33] (available in the ORCA package) were used in the calculations. Different active spaces were used in the calculations. The minimal active space was chosen to contain six MOs (five 5d orbitals of rhenium ion and one virtual orbital of *o*-benzoquinone) and 4 electrons. The maximal active space was chosen to contain nine MOs (five 5d orbitals of rhenium ion and HOMO, LUMO and two more virtual orbitals of *o*-benzoquinone) and 6 electrons. The resolution of identity approximation with corresponding correlation fitting of the basis set[34] was employed in order to speed up the calculations. Spin−orbit coupling was taken into account using the mean-field approximation (SOMF) as implemented in the ORCA package.[35] The effective Hamiltonian approach is used in order to extract the spin-Hamiltonian parameters.

The CASSCF wave functions of complex **1** were also used to calculate temperature dependence of its molar magnetic susceptibility. In these calculations, both the SOC and Zeeman effects are taken into account by diaganalization of the matrix

DOI: 10.1021/acs.inorgchem.5b00407
Inorg. Chem. 2015, 54, 6727−6735

$$\left\langle \Psi_I^{SM_S}|\hat{H}_{BO} + \hat{H}_{SOC} + \hat{H}_Z|\Psi_J^{S'M_S'}\right\rangle = \delta_{IJ}\delta_{SS'}\delta_{M_SM_S'}E_I^S + \left\langle \Psi_I^{SM_S}|\hat{H}_{SOC} + \beta\vec{B}(\hat{\vec{L}} + g_e\hat{\vec{S}})|\Psi_J^{S'M_S'}\right\rangle \quad (3)$$

in the basis of all computed CASSCF states $|\Psi_J^{S'M_S'}\rangle$. Magnetic susceptibility of each magnetic sublevel is computed numerically as the second derivative of the energy with respect to the magnetic field. The molar magnetic susceptibility is computed as averaged according to Boltzmann statistics. In order to reproduce powder measurement, the averaging over sphere for directions of magnetic field has been performed. Described treatment realized in the ORCA package[30] takes into account mixing of states due to both the spin−orbit coupling and magnetic field up to infinite order of perturbation theory meaning that the TIP correction and higher order corrections are already present in computed susceptibility. This treatment does not employ the spin-Hamiltonian formalism and can be used even for orbitally degenerate ground state.

The geometry of **1** for calculations was used from the X-ray data collected at 290 K. In most of the calculations, the phenyl groups were replaced by methyl ones, and ^{t}Bu groups were replaced by hydrogen atoms, the new structure was not optimized. The typical CH bond lengths of 1.08 Å were used for the dioxolene ligand. The P-CH_3 bond lengths were chosen to be equal to those of P−C bond lengths in **1** (about 1.79 Å) and the typical CH bond lengths of 1.096 Å were used for CH_3 groups.

A series of calculations for the X-ray geometry of **1** has also been performed using the CASSCF/SO-RASSI/SINGLE-ANISO procedure[36] implemented to the MOLCAS 7.6 program package.[37] Minimal active space consisting of six orbitals (five 5d orbitals of rhenium ion and one virtual orbital of *o*-benzoquinone) and 4 electrons was used throughout. Wave functions and energies of the spin-multiplets were obtained by the SA-CASSCF(4,6) method[38] with ANO-RCC full-electron relativistic basis set[39] and Douglas-Kroll-Hess second-order Hamiltonian (DKH2). Fifteen quintet states (S=2) were mixed with 105 triplet (S=1) and 105 singlet (S=0) states via spin−orbit coupling in RASSI module.[40] In addition, state specific calculations were also performed to estimate relative energies of the lowest singlet, triplet and quintet states.

Moreover, the properties of both the quintet and triplet states of complex **1** were calculated using a DFT approach at the DKH2-UB3LYP[32,41] and DKH2-UPB86[42] levels with relativistically recontracted versions of the def2-TZVP basis sets (for atoms H − Ba)[33] and SARC basis set of the same quality for rhenium.[33]

RESULTS AND DISCUSSION

Synthesis, XRD Structure, and Redox and Spectroscopic Properties of Complex 1. Refluxing $[ReOCl_3(PPh_3)_2]$ with 3,5-di-*tert*-butyl-1,2-benzoquinone (3,5-DTBQ) in toluene produces a red-brown complex [(dioxolene)$Re(OPPh_3)Cl_3$] (**1**) as the main product. During the reaction, both Re and quinone undergo reduction, with one PPh_3 being lost and another converted into $OPPh_3$ in the coordination sphere of Re. The hypothetical sequence of events leading to the formation of **1** includes abstraction of the terminal oxo ligand by PPh_3 and oxidative addition of the 3,5-DTBQ to the coordinatively unsaturated Re^{III} intermediate followed by intramolecular charge transfer from Re^{III} to DTBQ with formation of a Re^{IV}−DTBSQ or Re^{V}−DTBCat moiety; formation of a delocalized structure also cannot be excluded.[7,22]

$$[ReOCl_3(PPh_3)_2] + \text{3,5-DTBQ} = [(\text{3,5-di-}tert\text{-}Bu_2C_6H_2O_2)Re(OPPh_3)Cl_3] + PPh_3$$

Figure 1 displays the room temperature XRD structure of complex **1** (comparison of the geometry at different temperatures is summarized in Figures S5 and S6, Supporting Information). The Re center has the expected distorted octahedral environment with *mer*-arrangement of three Cl ligands. It is worth observing that closely related complexes with benzyl, $[ReCl_3(PhCOCOPh)(PPh_3)]$, and with *β*-lapachone, $[ReCl_3(PPh_3)(C_{15}H_{14}O_3)]$ are *fac*-isomers.[20] Comparison of the geometry of the ligand in **1** at room temperature with that of free 3,5-DTBQ[43] shows an elongation of C═O bonds by ca. 0.09 Å with a tendency to averaging of C−C and C═C bond lengths within the ring (which, nevertheless, are still not equal) as a result of reduction of the quinone, leading to partial restoration of aromaticity in the C_6-ring. The C(O)−C(O) bond length (1.412(10) Å) and the C−O distances (1.310(9) and 1.308(9) Å) are at the borderline between the typical values for Cat and SQ complexes.[9] In the catecholate complex $(Et_4N)(Et_3NH)[Re^{IV}Cl_4(Cat)]\cdot H_2Cat$,[21a] the Re−O bonds (2.0179(16) and 2.0275(15) Å) are noticeably longer than in complex **1** (1.963(6) and 1.939(5) Å), while the CO−CO bond length is close to that found in **1** (1.403(3) vs 1.412(10) Å). In the structure of **1** at 150 K, these values are 1.428(11) Å (CO−CO), 1.318(9) Å, and 1.320(10) Å (C−O), which demonstrates changing of the bond distances during cooling (full comparison presented in Table 1).

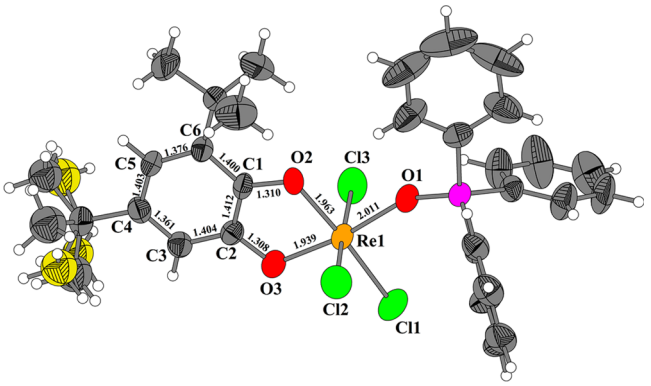

Figure 1. XRD structure of complex **1** (thermal ellipsoids in 50% probability) recorded at 293 K. Disordering of one tBu group is depicted in yellow.

The IR spectrum of **1** shows a strong band at 1438 cm^{-1} (Figure S7, Supporting Information) that is typically regarded as diagnostic of the SQ type complex.[44] VT-FTIR spectra (70−300 K) show retention of all peaks in a whole IR spectral region, and no additional C−O bands due to a change in the ligand and rhenium oxidation state were observed (Figure S7, Supporting Information).

Thus, the bonding situation in **1** is similar to that in the *β*-lapachone complex, $[ReCl_3(PPh_3)(C_{15}H_{14}O_3)]$, which was assigned[20] to a complex of Re(IV) coordinated to a 1,2-naphthosemiquinone radical.

The valence tautomeric transitions due to an electron transfer between metal cation and redox-active ligand are well-known for the metal−dioxolene complexes.[45] This phenomenon was first discovered for an octahedral cobalt complex,[46] and it is now well established for many 3d metal complexes.[45b] In order to check the possibility of thermally induced conversion between semiquinone (Re(IV) and 3,5-DTBSQ), catecholate (Re(V) and 3,5-DTBCat), and quinone (Re(III) and 3,5-

DOI: 10.1021/acs.inorgchem.5b00407
Inorg. Chem. 2015, 54, 6727−6735

Table 1. Selected Bond Lengths (Å) in the XRD Structures and an Empirical "Metrical Oxidation State" (MOS) of Dioxolene Ligands Calculated According to Ref [23] for Complex 1 Measured at 293 and 150 K and for Other Reported Rhenium Complexes

Bond	*d*, Å (293 K)	*d*, Å (150 K)	*d*,[a] Å Re^{IV}–SQ	*d*,[b] Å Re^{V}–Cat	*d*,[c] Å Re^{IV}–Cat
Re(1)–Cl(1)	2.301(2)	2.318(2)	2.3212		2.361
Re(1)–Cl(2)	2.307(3)	2.331(2)	2.3726		2.365
Re(1)–Cl(3)	2.334(3)	2.352(2)	2.3194		2.350
Re(1)–O(1)	2.011(5)	2.014(5)			2.337 (Re–Cl)
Re(1)–O(2)	1.963(6)	1.985(6)	2.011	2.041	2.028
Re(1)–O(3)	1.939(5)	1.956(5)	2.013	2.062	2.018
C(1)–O(2)	1.310(9)	1.318(9)	1.298	1.342	1.360
C(2)–O(3)	1.308(9)	1.320(10)	1.290	1.333	1.354
C(1)–C(2)	1.412(10)	1.428(11)	1.440	1.401	1.403
C(2)–C(3)	1.404(11)	1.417(11)	1.410	1.411	1.382
C(3)–C(4)	1.361(12)	1.368(12)	1.371	1.399	1.385
C(4)–C(5)	1.403(11)	1.433(12)	1.482	1.349	1.389
C(5)–C(6)	1.376(11)	1.376(12)	1.393	1.385	1.390
C(6)–C(1)	1.400(10)	1.412(11)	1.444	1.372	1.382
MOS	−1.5 ± 0.1	−1.4 ± 0.1	−1.0 ± 0.2	−2.1 ± 0.2	−2.0 ± 0.1

[a]Results for the $[Re^{IV}Cl_3(SQ)PPh_3]$ complex;[20] [b]Results for catechol ligand at equatorial position of the $[Re^{V}O(cat)_2PPh_3]^{2-}$ complex;[47] [c]Results for the $[Re^{IV}Cl_4(Cat)]^{2-}$ complex.[21a]

DTBQ) forms, the crystal structure of **1** was measured also at 150 K (Figure S6, Supporting Information). Table 1 displays characteristic bond lengths for structures of **1** at different temperatures, as well as bond distances for reported Re^{IV}–SQ,[20] Re^{V}–Cat,[47] and Re^{IV}–Cat[21a] complexes.

Table 1 demonstrates that most temperature changes of the bond lengths for complex **1** do not exceed 0.02 Å, although some of them are out of the error limits. Note that the low-temperature structure has slightly less alternated bonds in the phenyl ring of the dioxolene ligand, which is usually interpreted as increasing the presence of a cateholate form.[9] However, the results of our high-level *ab initio* calculations, VT-NMR, and VT-IR (see below) contradict this assumption.

As mentioned in the Introduction, an empirical "metrical oxidation state" (MOS) for the noninnocent ligands has recently been proposed.[23] Using a simple procedure of ref 23, we calculated values of MOS for complex **1** and for known complexes of rhenium with dioxolene type ligands (Table 1). Table 1 demonstrates that, for known rhenium complexes, the values of MOS are in perfect agreement with proposed valence-localized structures; viz., MOS is close to −1 for the Re(IV)–SQ complex[20] and MOS is close to −2 for cateholate complexes of Re(IV)[21a] and Re(V).[48] However, the values of MOS were found to be around −1.5 for complex **1** at both temperatures. Similar noninteger MOS values were reported by Brown for high-valent complexes of V(V) and Mo(VI) with catecholate and amidophenoxide ligands, and the effect was assigned to ligand-to-metal π bonding.[23] The origin of the noninteger MOS of the dioxolene ligand in **1** will be discussed along with results of the quantum chemical calculations (see the following section).

The NMR spectra (^1H, ^{13}C, ^{31}P) of **1** in $CDCl_3$ solution show the presence of paramagnetic species, as evidenced by a very large range of ^1H resonance shifts (Figure S8) and very broad ^{13}C and ^{31}P signals. The ^{31}P chemical shift (32 ppm with the line width of 35 Hz) for a solution of **1** is close to the signal of a free $OPPh_3$ molecule (29 ppm).[48] VT-NMR measurements (300–223 K) did not show any significant changes, except temperature dependent drift, over the whole scanned window.

Cyclic voltammetry of **1** in acetonitrile solution on a glassy carbon electrode in 0.05 M Bu_4NPF_6 + CH_3CN (Figure 2)

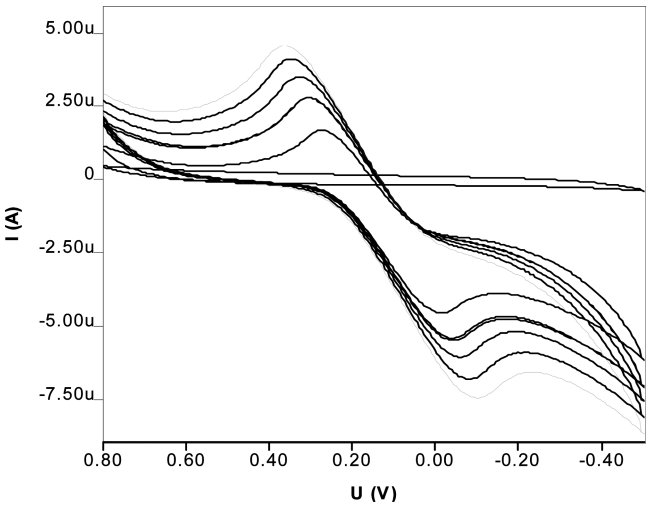

Figure 2. Cyclic voltammograms of **1** (15 mg/10 mL CH_3CN, 0.05 M Bu_4NPF_6 as background electrolyte) on a glassy carbon electrode. Scan route: 0.8 → −0.5 → 0.8 V. ν = 0.05; 0.10, 0.15, 0.20, and 0.25 V/s.

shows a fully reversible one-electron reduction process. The peak currents are proportional to the scan rate. For both the cathodic and anodic processes, the peak current I_p is linearly related to the square root of the scan rate ($I_p^c = -10.25\nu^{1/2} - 1.99$ and $I_p^a = 10.03\nu^{1/2} - 0.66$, see Table S4) with high correlation coefficients ($R^2 > 0.99$), which means that the electrochemical conversions of **1** on the glassy carbon electrode are diffusion-controlled. The reduction potential (ΔE_p) is 0.268 V at the scan rate 100 mV/s.

The electrochemical behavior of dioxolene complexes exhibits, according to the localized-valence model, a series of dioxolene-localized redox couples, which might be flanked with metal-localized couples.[7,13a] For example, complex [DBSQRe-$(CO)_4$] has two potentials: irreversible at −0.51 V (DBCat to DBSQ) and reversible at +0.43 V (DBSQ to DBQ) vs Fc/Fc^+.[49] The electrochemical process observed for complex **1** corresponds to one electron reduction of the delocalized ground state; thus, it cannot be assigned to a metal or ligand centered process.

DOI: 10.1021/acs.inorgchem.5b00407
Inorg. Chem. 2015, 54, 6727–6735

Figure 3 displays the electronic absorption spectrum of complex **1** in the CH_2Cl_2 solution. In the visible region, there

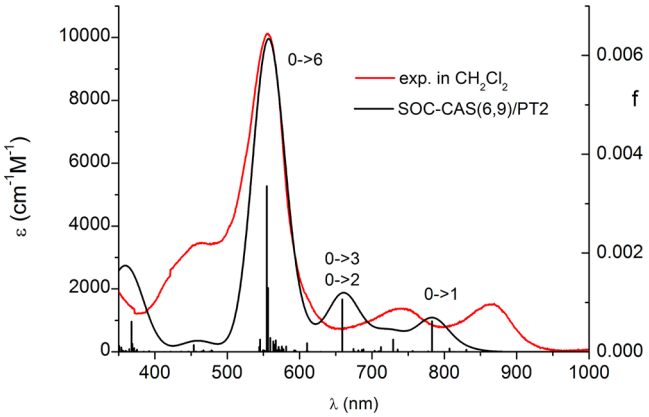

Figure 3. Experimental electronic absorption spectrum of complex **1** in CH_2Cl_2 (red spectrum). Black bars = positions of electronic transitions and their oscillator strengths calculated at the SOC-CASSCF(6,9)/NEVPT2 level, taking into account 5 quintet, 22 triplet, and 25 singlet states of modified complex **1** with ^{t}Bu groups replaced by hydrogen atoms and phenyl groups replaced by methyl ones. The black curve is a simulation of the calculated spectrum using a Gaussian shape of individual electronic transitions with a width of 50 nm.

are four bands with maxima at 465, 555, 740, and 865 nm. The most intense band at 555 nm has $\varepsilon = 10^4$ M^{-1} cm^{-1}. In the complex with β-lapachone, $[ReCl_3(PPh_3)(C_{15}H_{14}O_3)]$, the most intense charge-transfer band at 621 nm has a similar extinction coefficient ($\varepsilon = 1.08 \times 10^4$ M^{-1} cm^{-1}).[20] The origins of the electronic transitions corresponding to the absorption bands shown in Figure 3 have been assigned on the basis of *ab initio* calculations (see the following section).

Ab Initio Calculations of the Electronic Structure, Magnetic Properties, and Spectroscopy of Complex 1. In order to understand in detail the electronic structure and properties of **1**, we have performed high-level *ab initio* calculations using CASSCF and CASSCF/NEVPT2 procedures. Because rhenium has a very large spin−orbit coupling (SOC) constant, a relativistic DKH2 Hamiltonian[45] and nonperturbative approach to account for SOC has been employed. First, we performed the CASSCF(4,6) calculations with minimal active space consisting of 4 electrons and 6 molecular orbitals composed of five rhenium 5d-orbitals and the LUMO of *o*-quinone (Figure S1, SI). The room temperature structure of **1** (Figure 1) was used in the calculations. According to the state specific CASSCF(4,6)/ANO-RCC-VDZ calculations, the triplet state is a ground state of **1**. The quintet state is the first excited state at the energy level 0.38 eV (3060 cm^{-1}). The second excited state is a singlet state lying 1.36 eV (10940 cm^{-1}) above the ground state. The details of the calculations are presented in the SI.

In order to account for dynamic electron correlation and, thus, to achieve more accurate results, the SA-CASSCF/NEVPT2 procedure followed by SOC calculations with the larger TZVP-DKH basis set has been employed. Because this involved very resource-consuming procedures, we had to modify the structure of **1** and replaced the phenyl groups by methyl ones in the $OPPh_3$ ligand and ^{t}Bu groups by H atoms in the dioxolene ligand. Both minimal (4 electrons, 6 orbitals) and enlarged (up to 8 electrons and 10 orbitals) active spaces were used, and similar results were obtained in all cases. Therefore, only results obtained in the state averaged SOC-CASSCF(6,9)/NEVPT2 calculations with account of 5 quintet, 22 triplet, and 25 singlet states are representative.

Figure 4 displays the MOs involved in the active space for the representative calculations. The splitting of d-orbitals is typical

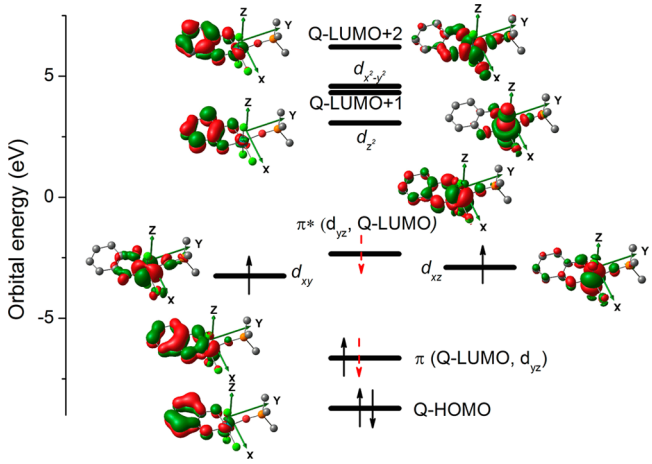

Figure 4. Molecular orbitals involved in the active space for the CASSCF(6,9)/TZVP-DKH calculations. The geometry corresponds to the room temperature XRD structure of **1** with phenyl groups replaced by methyl ones and tBu groups replaced by hydrogen atoms (the hydrogens are omitted for simplicity). The red dashed arrows represent the active MOs populations, which are significantly less than unity in the ground triplet state.

of octahedral complexes with large 10 Dq parameters characteristic for 5d transition metals. The d_{yz} orbital is strongly mixed with the *o*-quinone LUMO orbital, yielding bonding (π) and antibonding (π^*) combinations (Figure 4). The *o*-quinone LUMO orbital contributes mainly (~75%) to the bonding π-MO (~15% of d_{yz}). On the contrary, the contribution of metal d_{yz} (~71%) prevails in the antibonding π^*-MO (~18% of LUMO). The low-lying bonding π-MO provides a channel for the charge transfer to the dioxolene ligand.

Analysis of the electronic properties of the ground triplet state demonstrates that three configurations contribute mainly to its CASSCF wave function (Figure 5). Thus, the triplet state

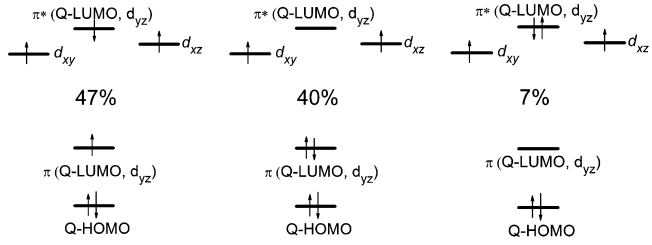

Figure 5. Occupations of the active orbitals in the configurations contributing mainly to the wave function of the triplet ground state.

wave function has a strongly multireference character and corresponds to a superposition of $Re^{IV}-SQ$ and $Re^{V}-Cat$ forms with comparable contributions although the $Re^{IV}-SQ$ state still predominates (>54%). Therefore, **1** can be formally classified as a Re^{IV} complex with the SQ form of the ligand although the electronic structure of **1** in its ground triplet state is more accurately described as a "mixed-valence complex" with the

DOI: 10.1021/acs.inorgchem.5b00407
Inorg. Chem. 2015, 54, 6727−6735

"mixed oxidation state" of rhenium.[50] The spin population at Re is predicted to be 2.23 and −0.37 at the dioxalene ligand, in excellent agreement with the calculations for the full structure of Figure 1 (Figure S2, SI).

Note that the "mixed-valence" nature of complex **1** coincides well with a noninteger value of MOS (−1.5 ± 0.1, Table 1). As a matter of fact, both effects, the multireference nature of the wave function and ligand-to-metal π bonding,[23] make comparable contributions to the highly delocalized electronic structure of the triplet ground state of **1** characterized by a MOS intermediate between those for complexes with unambiguous oxidation states (−1 for M−SQ and −2 for M−Cat). Unfortunately, we cannot quantitatively gauge the relative importance of the two effects.

The first exited state of **1** is predicted to be a quintet state with the relative energy 0.71 eV (or 5750 cm^{-1}) above the ground state, and in contrast to the ground state, its CASSCF wave function consists mainly of a single configuration that corresponds to the $Re^{IV}-SQ$ state (≥93%, with doubly occupied Q-HOMO while the other orbitals presented in Figure 5 are singly occupied). The energy difference between the ground triplet state and the first exited quintet state cannot be interpreted as an exchange coupling because it involves a large contribution from the charge transfer (metal-to-ligand) process. The spin population at Re in the quintet state is 2.75 at the CASSCF level, with the spin population at the SQ radical anion being 1.07.

Similar to the ground triplet state, the wave function of the lowest singlet state has a strongly multireference character and corresponds to a superposition of four configurations with comparable contributions, and the only difference is in that one of the almost degenerate d_{xz} and d_{xy} orbitals becomes doubly occupied (Figure S3, Supporting Information). The computed relative energy of this state is 1.04 eV or 8400 cm^{-1}.

To explain the EPR and magnetic susceptibility measurements, the spin−orbit coupling (SOC) was also taken into account in the SOC-CASSCF(6,9)/NEVPT2 calculations. Account of the SOC leads to the splitting of all spin multiplets, wherein three levels arising from the ground triplet state remain well separated from the higher-lying five states arising from the quintet excited state. Thus, the lowest three states can be assigned to a pseudospin $S = 1$ with splitting described by ZFS parameters D and E. These ZFS parameters and g-tensor were also calculated at both the SOC-CASSCF and SOC-CASSCF/NEVPT2 levels. In both cases the g-factor was found to be almost isotropic with g_{iso} equal to 1.78 and 1.77, respectively.

Taking into account spin−orbit coupling leads at both levels of calculations to anomalously large zero-field splitting of the ground state with pseudospin $S = 1$, $D = 341$ cm^{-1}, and $E/D = 0.019$ at the SOC-CASSCF level, and even larger splitting ($D = 481$ cm^{-1} and $E/D = 0.026$) at the SOC-NEVPT2 level. Analysis of the results demonstrates that the largest positive contribution to the D value (667 cm^{-1}) arises from the singlet state where one of the quasi degenerate orbitals d_{xz} or d_{xy} is doubly occupied and the ratio of the $Re^{IV}-SQ$ and $Re^{V}-Cat$ configurations is almost the same as in the ground triplet multiplet.

We have succeeded in accounting for both the spin−spin coupling (SSC) and SOC in the framework of the CASSCF/MRCI procedure,[30] also available in the ORCA suite of programs. As expected for a 5d-metal complex, the SSC contribution to the ZFS was found to be negligible (~0.2 cm^{-1} or 0.05%).

Account of the SOC leads also to the splitting of all exited quintet and triplet states of **1**. We roughly estimated the ZFS parameter D for the first excited state (with pseudospin $S = 2$) as ~100 cm^{-1}. This value is much smaller than that for the ground state and is typical of the rhenium complexes.[21a24d]

Figure 6 displays the temperature dependence of the molar magnetic susceptibility, $\chi(T)$, plotted as a product $\chi(T) \times T$. It

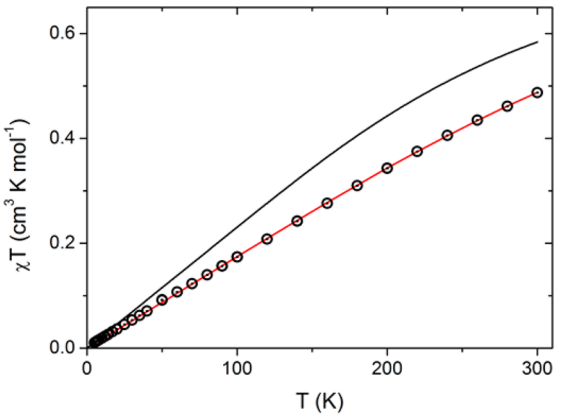

Figure 6. Experimental temperature dependence of the molar magnetic susceptibility of **1** measured at 5 kOe magnetic field (black circles); the best fitting using the spin-Hamiltonian as described in the text (red curve) and the directly computed magnetic susceptibility from the SOC-CASSCF(6,9)/NEVPT2 calculations taking into account 5 quintets, 22 triplets, and 25 singlets for the modified complex **1** with phenyl groups replaced by methyl ones and ^{t}Bu groups replaced by hydrogen (black curve).

is seen that this dependence is close to linear, which is typical of compounds exhibiting temperature-independent (second order) paramagnetism (TIP). This phenomenon is well-known for transition metal complexes[51] including Re(III) complexes with a diamagnetic ground state[52] and Re(II) complexes with a Kramers doublet ground state.[53] In the latter case, both types of paramagnetism, temperature dependent and temperature-independent, are observed.

In fact, the value of $\chi(T)$ for complex **1** slightly decreases with increasing temperature from 1.8×10^{-3} at 5 K to 1.6×10^{-3} cm^3/mol at 300 K. Most importantly, the temperature dependence of the magnetic susceptibility calculated at the SOC-CASSCF(8,9)/NEVPT2/def2-TZVP-DKH level (Figure 6, black curve) coincides fairly well with experiment. As described in the computational details, the treatment employed takes into account mixing of states due to SOC and magnetic field up to infinite order of perturbation theory. Thus, both the temperature dependent paramagnetism characteristic of the triplet ground state species with large ZFS and the TIP correction are already present in the computed susceptibility.

As presented above, the results of our calculations can also be interpreted using the spin-Hamiltonian approach; namely, complex **1** is characterized by pseudospin $S = 1$, an almost isotropic g-tensor, and very large ZFS. Thus, we simulated the temperature dependence of χT using the spin-Hamiltonian approach and two models described in the experimental and computational details, viz. two spin centers $S = {}^3/_2$ (Re^{IV} with ZFS) and $S = {}^1/_2$ (SQ) coupled by exchange interaction (J) in model 1, and one spin-center with $S = 1$ with ZFS in model 2. The use of both models and, hence, spin-Hamiltonians 1 and 2 leads to the same fitting (red curve) with the following parameters: $J = -1024$ cm^{-1}, $D(Re^{IV}) = 572$ cm^{-1}, $E/D = 0.25$,

DOI: 10.1021/acs.inorgchem.5b00407
Inorg. Chem. 2015, 54, 6727−6735

and $g(Re^{IV})$ = 1.94 for model 1 and D = 816 cm^{-1}, E/D = 0.31, g = 1.93 for model 2. Thus, simulation of the temperature dependence using the conventional spin-Hamiltonian approach leads to a very large value of the ZFS parameter D, even larger than the D value predicted in our calculations (481 cm^{-1} at highest level available). The value of J = −1024 cm^{-1} obtained in the first model corresponds to the energy difference between the excited quintet and ground triplet states being 4100 cm^{-1}. This value coincides well with the energy difference of 5750 cm^{-1} predicted by the CASSCF(8,9)/NEVPT2 calculations. Thus, based on a reasonable agreement between spin-Hamiltonian parameters (D and J) calculated using quantum chemistry and extracted from the analysis of $\chi(T)$, we can conclude that the main contribution to the magnetic susceptibility of complex **1** arises from the ZFS of the ground triplet state. However, some small TIP contribution cannot be excluded.

Figure 3 demonstrates that the electronic absorption spectrum of complex **1** in solution (red curve) is also reasonably well reproduced by the calculations at the same level of theory (SOC-CASSCF(8,9)/NEVPT2, black curve). Note that both the catecholate and semiquinonate complexes feature the electronic absorption spectra, which extend up to 1000−1100 nm, with semiquinonate complexes usually having more intense absorption bands.[8] Absorption bands at about 650 and 350 nm in the spectra of the SQ complexes are usually assigned to intraligand transitions[8] due to the similarity with those of the free 3,5-di-*tert*-butyl-*o*-benzosemiquinone radical anion.[55] Other bands were proposed to have mainly LMCT or MLCT character.[8] We performed assignment of the electronic absorption spectrum of **1** (Figure 3) on the basis of our calculations. However, analysis is complicated by the multi-reference wave function of the ground state. Thus, we characterized electronic states by the occupation numbers of the active space orbitals (Figure S4, SI).

Figure 3 demonstrates that one electron transition has a major contribution to the most intense band at 555 nm. This transition corresponds to the electron promotion from the ground state to the 30th magnetic sublevel. The main contributions to this magnetic sublevel come from the sixth excited CASSCF triplet state (∼60%, T_6) and from the first excited quintet state (∼14%). Figure S4 (Supporting Information) demonstrates that excitation from the ground triplet (T_0) to T_6 leads mainly to the population of the π and π^* orbitals at the expense of significant depopulation of Q-HOMO (Figure 4). Recall that π and π^* are linear combinations of Q-LUMO and d_{yz} wherein Q-LUMO contributes mainly to π. Thus, the most intense absorption band at 555 nm is assigned to a combination of the Q-HOMO → π and LMCT (Q-HOMO → π^*) excitations.

Predicted bands in the 600−850 nm spectral range are hypsochromically shifted from the experimental bands. This could be due to insufficient accuracy of the calculations: lack of dynamical correlation, small basis sets, or the substitution of H for ^{t}Bu makes the dioxolene ligand more electropositive while the $OPMe_3$ ligand used in the model is more basic than $OPPh_3$. The band at 660 nm in the simulated spectrum should correspond to the experimental band at 740 nm. The major contribution to this band comes from electron promotion to the 18th magnetic sublevel consisting mainly of T_2 (43%) and T_3 (43%) states of CASSCF calculations (Figure S4, SI). Transitions to both T_2 and T_3 states lead to a significant increase in the π^* orbital population at the expense of the π-orbital depopulation. Thus, this band can be assigned to the LMCT transition.

The main contribution to the longest wavelength band comes from the transition to the 11th magnetic sublevel composed mainly of the T_1 CASSCF state. This transition is also accompanied by a significant ligand to metal charge transfer (LMCT) along with the $d_{xz} \rightarrow \pi^*$ excitation (see for details Table S1 in the SI).

As mentioned in the Introduction, DFT has been mostly used to calculate the properties of the metal complexes with potentially noninnocent ligands.[6d,22−24] Thus, we also performed DFT calculations for the quintet and triplet states of complex **1**. The molecular orbitals obtained in these calculations are qualitatively similar to that presented in Figure 4. In accord with high-level calculations, the triplet state was predicted to be a ground state with the quintet state being a first excited state. In the triplet state, two α-electrons occupy d_{xy} and d_{xz} orbitals similar to that presented in Figure 4. The α- and β-orbitals of π-type (Figure 4) are also occupied, while the α- and $\beta-\pi^*$-orbitals remain empty. Thus, the DFT wave function of the triplet state corresponds to one of the configurations presented in Figure 5; its contribution to the CASSCF wave function is about 40%. It should be noted that the DFT wave function of the triplet state is noticeably contaminated, with the $\langle \hat{S}^2 \rangle$ being 2.18 and 2.07 at the UB3LYP (hybrid DFT) and UBP86 (pure DFT) levels, respectively. Contamination of the quintet wave function is negligible ($\langle \hat{S}^2 \rangle$ = 6.01). The quintet−triplet splitting was calculated to be 7050 and 8730 cm^{-1} at the UB3LYP and UBP86 levels, respectively. These values are noticeably larger than the 5750 cm^{-1} predicted at the CASSCF/NEVPT2 level.

It is clear that DFT calculations cannot reproduce a mixed-valence nature of the triplet ground state of complex **1**. Nevertheless, one can explain at least qualitatively the delocalized electronic structure of complex **1** and the unusual value of MOS on the basis of DFT calculations due to the ligand-to-metal π bonding (Figure 4, π-orbital).

We also calculated the ZFS parameters for **1** at the UB3LYP level: D = −484.8 cm^{-1}, E/D = 0.19 for the triplet state and D = −230 cm^{-1}, D/E = 0.14 for the quintet state. It is seen that, in contrast to the high-level calculations, DFT predicts negative D values. At the same time, a very large absolute D value was correctly predicted by DFT.

It is well-known that time-dependent DFT with conventional functionals significantly underestimates the energies of the charge-transfer (CT) transitions.[56] Thus, we employed the double-hybrid B2PLYP functional[57] known to perform well for the calculations of the CT transitions.[58] Nevertheless, we were unable to reasonably reproduce the electronic absorption spectrum of **1** (Figure 3, λ_{max}^{exp} = 555, 740, 865 nm). The most intense transition was predicted at 783 nm; about an order of magnitude less intense transitions were calculated at 476 and 674 nm. In addition, two long wavelength transitions were calculated at 1110 and 1280 nm. Thus, time-dependent DFT is not appropriate for the calculations of the UV−vis spectrum of complex **1**.

CONCLUSION

Therefore, based on the high-level SOC-CASSCF/NEVPT2 calculations, we can conclude that complex [(3,5-di-*tert*-$Bu_2C_6H_2O_2$)Re($OPPh_3$)Cl_3] has a ground state characterized by a pseudospin $\tilde{S}$ = 1 with significant zero-field splitting. The triplet state wave function has a strongly multireference

DOI: 10.1021/acs.inorgchem.5b00407
Inorg. Chem. 2015, 54, 6727−6735

character and corresponds to a superposition of Re^{IV}–*DTBSQ* and Re^{V}–*DTBCat* forms with comparable contributions. Two effects, the multireference nature of the wave function and ligand-to-metal π bonding, contribute to the highly delocalized electronic structure of the triplet ground state of **1** characterized by a MOS (−1.5) intermediate between those for complexes with valence-localized structures. Note that DFT calculations can take into account only one effect—a ligand-to-metal π bonding. The excited quintet state, on the contrary, corresponds to the Re^{IV}–*DTBSQ* form and is predicted to have much higher energy. This energy difference cannot be interpreted as a consequence of exchange coupling between paramagnetic centers, Re(IV), and SQ radical anion, because of the delocalized mixed-valence nature of the ground state.

The results of the high-level ab initio calculations are in good agreement with the spectroscopic and magnetic properties of complex **1**. The temperature dependence of the magnetic susceptibility is well reproduced in the assumption of anomalously large ZFS in the ground triplet state of **1**. The latter effect is quantitatively predicted at high-level calculations, demonstrating the predominant contribution of the spin–orbit coupling to the ZFS. The electronic absorption spectrum of **1** is also fairly well reproduced by the high-level ab inition calculations, and all visible absorption bands were assigned as LMCT bands with significant contribution of the intraligand transition in the most intense band at 555 nm.

■ ASSOCIATED CONTENT

Supporting Information

Details of quantum chemical calculations, comparison in geometry between low and high temperature structures, X-ray data collection, VT-FTIR, ^{1}H NMR, and cif files. The Supporting Information is available free of charge on the ACS Publications website at DOI: 10.1021/acs.inorgchem.5b00407.

■ AUTHOR INFORMATION

Corresponding Authors

*E-mail: abramov@niic.nsc.ru.
*E-mail: gritsan@kinetics.nsc.ru.

Funding

This work was partially supported by RFBR grants (12-03-33028, 15-03-03242) and by a President of Russian Federation fellowship (P.A.A.).

Notes

The authors declare no competing financial interest.

■ ACKNOWLEDGMENTS

P.A.A. thanks S. V. Klementyeva (IOMC RAS, Nizhny Novgorod) for kindly providing us with a supply of 3,5-quinone. The authors thank M. Fedin (ESR experiments, International Tomographic Center), N.F. Zakharchuk (CV experiments), and N. I. Sheldyakova for VT-FTIR experiments (Nikolaev Institute of Inorganic Chemistry). This work was supported by RFBR grants 12-03-33028 and 15-03-03242, and by a President of RF grant SS-516.2014.3.

■ REFERENCES

(1) (a) Lemeire, M. T. *Pure Appl. Chem.* **2004**, *76*, 277–293. (b) Vostrikova, K. E. *Coord. Chem. Rev.* **2008**, *252*, 1409–1419.

(2) (a) Sigel, H. S. A. *Metalloenzymes involving Amino Acid Residue and Related Radicals*; Marcel Dekker, New York, 1994. (b) Stubbe, J.; Van der Donk, W. A. *Chem. Rev.* **1998**, *98*, 705–765.

(3) Kaim, W.; Schwederski, B. *Coord. Chem. Rev.* **2010**, *254*, 1580–1588.

(4) Lyaskovskyy, V.; de Bruin, B. *ACS Catal.* **2012**, *2*, 270–279.

(5) Dei, A.; Gatteschi, D.; Sangregorio, C.; Sorace, L. *Acc. Chem. Res.* **2004**, *37*, 827–835.

(6) (a) Butin, K. P.; Beloglazkina, Y. K.; Zyk, N. V. *Uspekhi Khim.* **2005**, *74*, 585–609. (b) Ward, M. D.; McCleverty, J. A. *J. Chem. Soc., Dalton Trans.* **2002**, 275–288. (c) Gorelsky, S. I.; Dodsworth, E. S.; Lever, A. B. P.; Vlček, A., Jr. *Coord. Chem. Rev.* **1998**, *174*, 469–494. (d) Ray, K.; Petrenko, T.; Wieghardt, K.; Neese, F. *Dalton Trans.* **2007**, 1552–1566. (e) Chirik, P. J. *Inorg. Chem.* **2011**, *50*, 9737–9740 (and other papers of this thematic issue). (f) Berben, L. A.; de Bruin, B.; Heyduk, A. F. *Chem. Commun.* **2015**, *51*, 53–54 (and other papers of this thematic issue).

(7) Pierpont, C. G.; Lange, C. W. *Prog. Inorg. Chem.* **1994**, *41*, 331–442.

(8) (a) Benelly, C.; Dei, A.; Gatteschi, D.; Pardi, L. *Inorg. Chem.* **1988**, *27*, 2831–2836. (b) Benelly, C.; Dei, A.; Gatteschi, D.; Gudel, H. U.; Pardi, L. *Inorg. Chem.* **1989**, *28*, 3089–3091. (c) Benelly, C.; Dei, A.; Gatteschi, D.; Pardi, L. *Inorg. Chem.* **1989**, *28*, 1476–1480. (d) Benelly, C.; Dei, A.; Gatteschi, D.; Pardi, L. *Inorg. Chem.* **1990**, *29*, 3409–3415.

(9) Vlček, A., Jr. *Comments Inorg. Chem.* **1994**, *16*, 207–228.

(10) Meyer, K. H. *Chem. Ber.* **1908**, *41*, 2568–2576.

(11) Clowley, P. J.; Haendler, H. M. *Inorg. Chem.* **1962**, *1*, 904–909.

(12) Eaton, D. R. *Inorg. Chem.* **1964**, *3*, 1268–1271.

(13) (a) Pierpont, C. G.; Buchanan, R. M. *Coord. Chem. Rev.* **1981**, *38*, 45–87. (b) Pierpont, C. G. *Coord. Chem. Rev.* **2001**, *216*, 99–125. (c) Chang, H.-C.; Ishii, T.; Kondo, M.; Kitagawa, S. *J. Chem. Soc., Dalton Trans.* **1999**, 2467–2476. (d) Jung, O.-S.; Jo, D. H.; Lee, Y.-A.; Conklin, B. J.; Pierpont, C. G. *Inorg. Chem.* **1997**, *36*, 19–24. (e) Da Silva, R. S.; Gorelsky, S. I.; Dodsworth, E. S.; Tfouni, E.; Lever, A. B. P. *J. Chem. Soc., Dalton Trans.* **2000**, 4078–4088. (f) Lever, A. B. P.; Masui, H.; Metcalfe, R. A.; Stufkens, D. J.; Dodsworth, E. S.; Auburn, P. R. *Coord. Chem. Rev.* **1993**, *125*, 317–331. (g) Auburn, P. R.; Dodsworth, E. S.; Haga, M.; Liu, W.; Nevin, W. A.; Lever, A. B. P. *Inorg. Chem.* **1991**, *30*, 3502–3512. (h) Ward, M. D. *Chem. Soc. Rev.* **1995**, *24*, 121–134. (i) Caneschi, A.; Cornia, A.; Dei, A. *Inorg. Chem.* **1998**, *37*, 3419–3421.

(14) (a) Attia, A. S.; Pierpont, C. G. *Inorg. Chem.* **1998**, *37*, 3051–3056. (b) Bhattacharya, S.; Pierpont, C. G. *Inorg. Chem.* **1992**, *31*, 35–39. (c) Haga, M.; Dodsworth, E. S.; Lever, A. B. P. *Inorg. Chem.* **1986**, *25*, 447–453. (d) Bhattacharya, S.; Boone, S. R.; Fox, G. A.; Pierpont, C. G. *J. Am. Chem. Soc.* **1990**, *112*, 1088–1096. (e) Meacham, A. P.; Druce, K. L.; Bell, Z. R.; Ward, M. D.; Keister, J. B.; Lever, A. B. P. *Inorg. Chem.* **2003**, *42*, 7887–7896. (f) Speier, G.; Tisza, S.; Tyeklar, Z.; Lange, C. W.; Pierpont, C. G. *Inorg. Chem.* **1994**, *33*, 2041–2045. (g) Warncke, K.; Babcock, G. T.; Dooley, D. M.; McGuirl, M. A.; McCracken, J. *J. Am. Chem. Soc.* **1994**, *116*, 4028–4037. (h) Abakumov, G. A.; Garnov, V. A.; Nevodchikov, V. I.; Cherkasov, V. K. *Dokl. Akad. Nauk SSSR* **1989**, *304*, 107–111. (i) Zakharov, L. N.; Saf'yanov, Y. N.; Struchkov, Y. T.; Abakumov, G. A.; Cherkasov, V. K.; Garnov, V. A. *Koord. Khim.* **1990**, *16*, 802–810. (j) Kondo, M.; Hamafani, M.; Kitagawa, S.; Pierpont, C. G.; Unoura, K. *J. Am. Chem. Soc.* **1998**, *120*, 455–456. (k) Miyasaka, H.; Chang, H.-C.; Mochizuki, K.; Kitagawa, S. *Inorg. Chem.* **2001**, *40*, 3544–3554. (l) Chang, H.-C.; Mochizuki, K.; Kitagava, S. *Inorg. Chem.* **2005**, *44*, 3799–3809. (m) Chang, H.-C.; Mochizuki, K.; Kitagava, S. *Inorg. Chem.* **2005**, *44*, 3810–3817.

(15) Abakumov, G. A.; Lobanov, A. V.; Cherkasov, V. K.; Razuvaev, G. A. *Inorg. Chim. Acta* **1981**, *49*, 135–138.

(16) Cheng, C. P.; Wang, S. R.; Lin, J. C.; Wang, S.-L. *J. Organomet. Chem.* **1988**, *349*, 375–382.

(17) Reibenspies, J. H.; Draper, J. D.; Darensbourg, D. J. *Z. Kristallogr.* **1996**, *211*, 501–502.

(18) Lippert, C. A.; Soper, J. D. *Inorg. Chem.* **2010**, *49*, 3682–3684.

DOI: 10.1021/acs.inorgchem.5b00407
Inorg. Chem. 2015, 54, 6727–6735

(19) DeLearie, L. A.; Pierpont, C. G. *J. Am. Chem. Soc.* **1986**, *108*, 6393−6394.
(20) Sokolov, M. N.; Fyodorova, N. E.; Paetow, R.; Fenske, D.; Ravelo, A. G.; Naumov, D.; Yu; Fedorov, V. E. *Inorg. Chim. Acta* **2007**, *360*, 2192.
(21) (a) Cuevas, A.; Geis, L.; Pintos, V.; Chiozzone, R.; Sanchíz, J.; Hummert, M.; Schumann, H.; Kremer, C. *J. Mol. Struct.* **2009**, *921*, 80−84. (b) Pintos, V.; Cuevas, A.; Onetto, S.; Seoane, G.; Denis, P. A.; Gancheff, J. S.; Faccio, R.; Mombrú, A. W.; Kremer, C. *J. Mol. Struct.* **2010**, *963*, 9−15.
(22) Budzelaar, P. H. M.; de Bruin, B.; Gal, A. W.; Wieghardt, K.; van Lenthe, J. P. H. *Inorg. Chem.* **2001**, *40*, 4649−4655.
(23) Brown, S. N. *Inorg. Chem.* **2012**, *51*, 1251−1260.
(24) (a) Rodriguez, J. H.; Wheeler, D. E.; McCusker. *J. Am. Chem. Soc.* **1998**, *120*, 12051−12068. (b) Ingram, J. D.; Costa, P. J.; Adams, H.; Ward, M. D.; Felix, V.; Thomas, J. A. *Inorg. Chem.* **2012**, *51*, 10483−10494. (c) Touron Touceda, P.; Mosquera Vazquez, S.; Lima, M.; Lapini, A.; Foggi, P.; Dei, A.; Righini, R. *Phys. Chem. Chem. Phys.* **2012**, *14*, 1038−1047. (d) Martinez-Lillo, J.; Mastropietro, T. F.; Lhotel, E.; Paulsen, C.; Cano, J.; De Munno, G.; Faus, J.; Lloret, F.; Julve, M.; Nellutla, S.; Krzystek, J. *J. Am. Chem. Soc.* **2013**, *135*, 13737−13748. (e) Yumata, N. C.; Habarurema, G.; Mukiza, J.; Gerber, T. I. A.; Hosten, E.; Taherkhani, F.; Nahali, M. *Polyhedron* **2013**, *62*, 89−103.
(25) (a) Neese, F. *Coord. Chem. Rev.* **2009**, *253*, 526−563. (b) Atanasova, M.; Aravena, D.; Suturina, E.; Bill, E.; Maganas, D.; Neese, F. *Coord. Chem. Rev.* **2015**, *289*−*290*, 177−214.
(26) Johnson, N. P.; Lock, C. J. L.; Wilkinson, G. *J. Chem. Soc.* **1964**, 1054−1066.
(27) Sheldrick, G. *Acta Crystallogr., Ser. A* **2008**, *64*, 112−122.
(28) Kalinnikov, V. T.; Rakitin, Yu. V. Introduction in Magnetochemistry. *Method of Static Magnetic Susceptibility*; Nauka: Moscow, 1980; p 302 (in Russian).
(29) Bill, E. Unpublished result. The JulX program package can be requested by e-mail eckhard.bill@cec.mpg.de.
(30) (a) Neese, F. *Wires Comput. Mol. Sci.* **2012**, *2*, 73−78. (b) Neese, F.; with contributions from Becker, U.; Ganyushin, G.; Hansen, A.; Izsak, R.; Liakos, D. G.; Kollmar, C.,; Kossmann, S.; Pantazis, D. A.; Petrenko, T.; Reimann, C.; Riplinger, C.; Roemelt, M.; Sandhöfer, B.; Schapiro,I.; Sivalingam, K.; Wennmohs, F.; Wezisla, B.; Kállay, M.; Grimme, S.; Valeev, E. *ORCA—An ab initio, DFT and semiempirical SCF-MO package*, Version 3.0; Mülheim a.d.R., 2013.
(31) (a) Angeli, C.; Cimiraglia, R.; Evangelisti, S.; Leininger, T.; Malrieu, J.-P. *J. Chem. Phys.* **2001**, *114*, 10252−10264. (b) Angeli, C.; Cimiraglia, R.; Malrieu, J.-P. *Chem. Phys. Lett.* **2001**, *350*, 297−305. (c) Angeli, C.; Cimiraglia, R.; Malrieu, J.-P. *J. Chem. Phys.* **2002**, *117*, 9138−9153.
(32) Hess, B. A. *Phys. Rev. A* **1986**, *33*, 3742−3748.
(33) Pantazis, D. A.; Chen, X. Y.; Landis, C. R.; Neese, F. *J. Chem. Theory Comput* **2008**, *4*, 908−919.
(34) Neese, F. *J. Comput. Chem.* **2003**, *24*, 1740−1747.
(35) Ganyushin, D.; Neese, F. *J. Chem. Phys.* **2013**, *138*, 104113.
(36) (a) Roos, B. O.; Malmqvist, P.-A. *Phys. Chem. Chem. Phys.* **2004**, *6*, 2919−2927. (b) Malmqvist, P.-A.; Roos, B. O.; Schimmelpfennig, B. *Chem. Phys. Lett.* **2002**, *357*, 230−240. (c) Chibotaru, L. F.; Ungur, L. *J. Chem. Phys.* **2012**, *137*, 064112.
(37) Aquilante, F.; De Vico, L.; Ferre, N.; Ghigo, G.; Malmqvist, P.-A.; Neograd y, P.; Pedersen, T. B.; Pitoňak, M.; Reiher, M.; Roos, B. O.; Serrano-Andres, L.; Urban, M.; Veryazov, V.; Lindh, R. *J. Comput. Chem.* **2010**, *31*, 224−247.
(38) (a) Malmqvist, P.-A.; Roos, B. O. *Chem. Phys. Lett.* **1989**, *155*, 189−194. (b) Andersson, K.; Roos, B. O. *Chem. Phys. Lett.* **1992**, *191*, 507−514. (c) Pierloot, K. *Mol. Phys.* **2003**, *101*, 2083−2094. (d) Roos, B. O.; Andersson, K.; Fulscher, M. P.; Malmqvist, P.-A.; Serrano-Andres, L.; Pierloot, K.; Merchan, M. *Adv. Chem. Phys.* **1996**, *93*, 219−331.
(39) (a) Roos, B. O.; Lindh, R.; Malmqvist, P.-A.; Veryazov, V.; Widmark, P. O. *J. Phys. Chem. A* **2004**, *108*, 2851−2858. (b) Roos, B. O.; Lindh, R.; Malmqvist, P.-A.; Veryazov, V.; Widmark, P. O. *J. Phys. Chem. A* **2005**, *109*, 6575−6579.
(40) Malmqvist, P.-A.; Roos, B. O.; Schimmelpfennig, B. *Chem. Phys. Lett.* **2002**, *357*, 230−240.
(41) (a) Becke, A. D. *J. Chem. Phys.* **1993**, *98*, 5648−5652. (b) Lee, C.; Yang, W.; Parr, R. G. *Phys. Rev. B* **1988**, *37*, 785−789.
(42) (a) Becke, A. D. *Phys. Rev. A* **1988**, *38*, 3098−3100. (b) Perdew, J. P. *Phys. Rev. B* **1986**, *33*, 8822−8824.
(43) Weiner, H.; Finke, R. G. *J. Am. Chem. Soc.* **1999**, *121*, 9831−9842.
(44) Lever, A. B. P.; Auburn, P. R.; Dodsworth, E. S.; Haga, M.; Liu, W.; Melnik, M.; Cand, W.; Nevin, A. *J. Am. Chem. Soc.* **1988**, *110*, 8076−8084.
(45) (a) Evangelio, E.; Ruiz-Molina, D. *Eur. J. Inorg. Chem.* **2005**, 2957−2971. (b) Tezgerevska, T.; Alley, K. G.; Boskovic, C. *Coord. Chem. Rev.* **2014**, *265*, 23−40.
(46) Buchanan, R. M.; Pierpont, C. G. *J. Am. Chem. Soc.* **1980**, *102*, 4951−4957.
(47) Kettler, P. B.; Chang, Y.-D.; Zubieta, J.; Abrams, M. J. *Inorg. Chim. Acta* **1994**, *218*, 157−165.
(48) Kühl, O. *Phosphorus-31 NMR spectroscopy*; Springer-Verlag: Berlin Heidelberg, 2008.
(49) Hartl, F.; Vlček, A., Jr. *Inorg. Chem.* **1992**, *31*, 2869−2876.
(50) Day, P.; Hush, N. S.; Clark, R. J. H. *Phil. Trans. A* 2008, V. *366* (issue 1862), 5−14 (and other papers of the same issue, Discussion Meeting Issue 'Mixed valency' organized by Robin J. H. Clark, Peter Day, and Noel S. Hush).
(51) Kahn, O. *Molecular magnetism*; VCH Publisher: New York, 1993; p 7.
(52) (a) Meyer, K.; Mindiola, D. J.; Caulton, K. G. *Angew. Chem., Int. Ed.* **2014**, *53*, 14139−14143. (b) Bouwkamp, M. W.; Lobkovsky, E.; Neese, F.; Wieghardt, K.; Chirik, P. J. *J. Am. Chem. Soc.* **2006**, *128*, 13901−13912. (c) Nguyen, T.; Sutton, A. D.; Brynda, M.; Fettinger, J. C.; Long, G. J.; Power, P. P. *Science* **2005**, *310*, 844−847.
(53) (a) Gunz, H. P.; Leigh, G. J. *J. Chem. Soc.* **1971**, 2229−2233. (b) Ozerov, O. V.; Watson, L. A.; Pink, M.; Baik, M.-H.; Caulton, K. G. *Organometallics* **2004**, *23*, 4934−4943.
(54) (a) Schelter, E. J.; Bera, J. K.; Bacsa, J.; Galan-Mascaros, J. R.; Dunbar, K. R. *Inorg. Chem.* **2003**, *42*, 4256−4258. (b) Dunbar, K. R.; Schelter, E. J.; Tsekerblat, B. S.; Ostrovsky, S. M.; Morovitsky, V. Y.; Palii, A. V. *Polyhedron* **2003**, *22*, 2545−2556. (c) Pacheko, M.; Gonzalez-Platas, J.; Faccio, R.; Lloret, F.; Julve, M.; Kremer, C. *Dalton Trans.* **2013**, *42*, 15361−15371.
(55) Stallings, M. D.; Morrison, M. M.; Sawyer, D. T. *Inorg. Chem.* **1981**, *20*, 2655−2660.
(56) Dreuw, A.; Head-Gordon, M. *Chem. Rev.* **2005**, *105*, 4009−4037.
(57) Grimme, S.; Neese, F. *J. Chem. Phys.* **2007**, *127*, 154116.
(58) (a) Di Meo, F.; Trouillas, P.; Adamo, C.; Sancho-Garcia, J. C. *J. Chem. Phys.* **2013**, *139*, 164104. (b) Semenov, N. A.; Lonchakov, A. V.; Pushkarevsky, N. A.; Suturina, E. A.; Korolev, V. V.; Lork, E.; Vasiliev, V. G.; Konchenko, S. N.; Beckmann, J.; Gritsan, N. P.; Zibarev, A. B. *Organometallics* **2014**, *33*, 4302−4314.

DOI: 10.1021/acs.inorgchem.5b00407
Inorg. Chem. 2015, 54, 6727−6735